Carbohydrate Polymers 225 (2019) 115214

Contents lists available at ScienceDirect

Carbohydrate Polymers

journal homepage: www.elsevier.com/locate/carbpol

Preparation of superabsorbent resin with fast water absorption rate based on hydroxymethyl cellulose sodium and its application

Sha Cheng, Xiaomei Liu, Jianghong Zhen, Ziqiang Lei*

Key Laboratory of Eco-functional Polymer Materials of the Ministry of Education, Key Laboratory of Eco-Environment Polymer Materials of Gansu Province, College of Chemistry and Chemical Engineering, Northwest Normal University, Lanzhou, 730070, China

ARTICLE INFO

Keywords:
Superabsorbent resin
Hydroxymethyl cellulose sodium
Water absorption
Swelling kinetic
Water evaporation in soil

ABSTRACT

To study the application of superabsorbent resin (SAR) in preventing water evaporation in soil, hydroxymethyl cellulose sodium-g-poly (acrylic acid-co-2- acrylamido-2-methyl-1-propanesulfonic acid)/laterite (NaHMC-g-P (AA-co-AMPS)/ laterite) was prepared by radical polymerization. The structure and morphology of SAR were characterized by FTIR, SEM and TGA. The factors affecting the water absorbency of SAR were studied and the water absorption of the resin under the optimum synthetic conditions reached the equilibrium at 15 min in distilled water, and the optimum water absorption of SAR was 1329 g/g, 269 g/g and 140 g/g in distilled water, tap water and 0.9 wt% NaCl solution, respectively. The swelling kinetic mechanism of the SAR was explained by the pseudo-second-order swelling kinetics model and Ritger-Peppas model. The effects of soil type, particle size and content of SAR on water evaporation rate in soil were studied.

1. Introduction

Superabsorbent resin (SAR) is a kind of functional polymer material with strong hydrophilic groups (Cheng, Liu, Yang, & Zhang, 2018) and three-dimensional network structure (Adair, Kaesaman, & Klinpituksa, 2017). It not only has excellent water absorption performance, but also has good water retention performance. Therefore, it is widely used in medicine and health (Demeter et al., 2017), food industry, water treatment (Li, Lu, Xiao, Gao, & Diao, 2013; Zhu, Bai, & Hou, 2017), agriculture and forestry (Cheng et al., 2018), urea fertilizer (He et al., 2017; Zhang, Liang, Yang, Liu, & Yao, 2014) and drug sustained release, chemical industry (Mechtcherine et al., 2018; Wang, Yang, Cheng, Wu, & Liang, 2015) and other fields. However, its application in preventing water evaporation in soil has been reported rarely.

Water evaporation in soil is a process in which water is transferred from liquid to gaseous to atmosphere. It is related to external meteorological conditions, such as temperature, humidity, wind speed and rainfall. Excessive or insufficient water in soil has certain effects on plants and microorganisms. (Guilherme et al., 2015) The irregular three-dimensional network structure of superabsorbent resin makes it has strong water absorption ability. It can repeatedly absorb hundreds or even thousands of times of water than its own weight (Hosseinzadeh & Ramin, 2016; Kang, Hong, & Moon, 2017). After water absorption, it expands into hydrogel and slowly releases water for crop absorption and utilization. It is an excellent drought-resistant and water-saving material. If the evaporation loss of water in soil can be restrained, especially in arid areas, it is of great significance to restrain evaporation, prolong the time of water in soil and improve the effective utilization of water. The use of superabsorbent resin is an important mean to achieve this goal.

Jun-Ping Zhang et al. studied recycling waste polyethylene film for amphoteric superabsorbent resin synthesis (Zhang and Zhang, 2018a). Graphene oxide/poly(acrylic acid-co-acrylamide) super-absorbent hydrogel nanocomposites was prepared by Yiwan Huang et al. (Huang et al., 2012). Shixin Fang et al. synthesized superabsorbent polymers based on chitosan derivative graft acrylic acid-co-acrylamide (Fang et al., 2019). Zhimin Wang et al. studied synthesis and swelling behaviors of carboxymethyl cellulose-based superabsorbent resin hybridized with graphene oxide (Wang et al., 2017). However, superabsorbent resin has some disadvantages, such as high production cost, poor degradability (Olad, Gharekhani, Mirmohseni, & Bybordi, 2017) and poor salt resistance. In addition, with the increase consumption of oil, coal (Qin et al., 2017) and other mineral resources, and the aggravation of environmental pollution, the preparation of low-cost, environmentally friendly and salt-resistant superabsorbent resins has become a hot topic for researchers.

The number of hydrophilic groups, three-dimensional network structure, gel strength, etc. in the superabsorbent resin all have an

* Corresponding author.
E-mail address: leizq@nwnu.edu.cn (Z. Lei).

https://doi.org/10.1016/j.carbpol.2019.115214
Received 10 May 2019; Received in revised form 13 August 2019; Accepted 19 August 2019
Available online 19 August 2019
0144-8617/

influence on the water absorption property, and the swelling absorption process is mainly controlled by chemical absorption. As an inorganic mineral, the introduction of laterite into superabsorbent resin, which can not only reduce the production cost, but also improve its swelling capacity, thermal stability and gel strength (Salmawi, El-Naggar, & Ibrahim, 2018). Cellulose, as a natural macromolecule compound, which has the advantages of low toxicity (Hosseinzadeh & Ramin, 2016), low cost, biodegradability, biocompatibility (Peng, Hu et al., 2016; Peng, Wang et al., 2016), etc. Moreover, it contains more active groups of molecular structure (e.g., hydroxyl group, ether bond, etc.), and many derivatives can be obtained by chemical reaction. Cellulose derivatives have many different functional groups and are more soluble in water (Bao, Ma, & Sun, 2012). Therefore, the introduction of cellulose derivatives can improve the water absorption and biodegradability of superabsorbent resins. At present, there are many reports about carboxymethyl cellulose (Capanema et al., 2018; Wang et al., 2017), but less information about other cellulose derivatives. The introduction of 2-acrylamide-2-methyl-1-propanesulfonic acid into the synthesis of superabsorbent resin can improve its salt tolerance (Zhu et al., 2017). Therefore, organic-inorganic composites containing cellulose derivatives and inorganic materials have broad development prospects.

In this paper, hydroxymethyl cellulose sodium (NaHMC), laterite and 2-acrylamide-2-methyl-1-propionicsulfonic acid were used as raw materials to prepare organic-inorganic composite superabsorbent resin by free radical copolymerization. And the swelling mechanism of the prepared product is also explained by the pseudo-second-order kinetics model and Ritger-Peppas model. In addition, superabsorbent resin was used to prevent water evaporation in soil. The effect of soil type, particle size and content of superabsorbent resin on evaporation performance in soil was investigated.

2. Experimental

2.1. Materials

Hydroxymethyl Cellulose Sodium (NaHMC, AR)was obtained from Shanghai Macklin Biochemical Co., Ltd., 2-Acrylamido-2-methyl-1-propanesulfonic acid (AMPS, AR) was obtained from Aladdin Reagent (Shanghai) Co., Ltd., acrylic acid (AA, AR) was obtained from Tianjin Damao Chemical Reagent Factory, sodium hydroxide (NaOH, AR) was obtained from Tianjin Yiwanda Chemical Co., Ltd., *N,N-m*ethylene-bis-acrylamide (MBA,CP) was obtained from Chinese Drug Group Chemical Reagent Co., Ltd., ammonium persulfate (APS, 98%) was obtained from Yantai Shuangshuang Chemical Co., Ltd. and secondary distilled water.

2.2. Preparation of NaHMC-g-P (AA-co-AMPS)/laterite SAR

Dispersion solution was prepared by adding 30 mL distilled water and NaHMC to 250 mL four-port flask with mechanical agitator. In continuous stirring, the solution was heated to 70 ℃ for 45 min. The reactant was cooled to 50 ℃ and 5 mL the aqueous solution of APS was added. After 10 min, the mixture containing partially neutralized acrylic acid, AMPS, cross-linker MBA and laterite was dripped into the above system. Then the temperature was slowly raised to 70 ℃, and the reaction for 3 h at constant temperature. Nitrogen was used to throughout the whole experimental process. After reaction, the product was soaked in absolute ethanol for 1 h, then washed with distilled water for 3 times. Then the product was put into the blast drying chamber and dried to constant weight at 60 ℃, then crushed and passed through sieve. The particle size of all resins used for testing is about 50 meshes.

The preparation of NaHMC-g-P (AA-co-AMPS) superabsorbent resin was in accordance with the above process except without laterite . The structure of Hydroxymethyl Cellulose Sodium and the reaction mechanism for synthesis of NaHMC-g-P (AA-co-AMPS)/laterite were shown in Schemes 1 and 2.

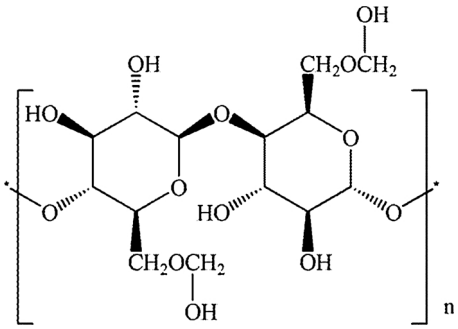

Scheme 1. Structure of Hydroxymethyl Cellulose Sodium.

2.3. Preparation of anti-evaporation material for clay-based superabsorbent resin

Put 700 g sand (Its function is to simulate the desertification area) into plastic boxes with the same specifications (20.5*13.2*6.5 cm), make the sand level in the plastic boxes, add 120 g distilled water, make the sand wet evenly. Then, 150 g clay (laterite, kaolin, attapulgite) or loess, and added 5 wt% straw powder of clay or loess and superabsorbent resin of different quality, 170 g distilled water was added, respectively. The mixture was stirred evenly at the rotational speed of 300 ~ 400 r/min, and then spread in the plastic box, respectively.

2.4. Characterization

The infrared spectra of NaHMC and prepared samples were recorded by using Digilab FTS-3000 Fourier-transform Infrared Spectrometer in the range of 4000-400 cm^{-1}. The solid sample and KBr were mixed and ground into powder with the mass ratio of 1:100 and transparent sheet was formed by pressing method.

The morphological changes of the samples were observed by Zeiss ULTRA plus thermal field emission scanning electron microscopy (SEM).

Thermal stability analysis (TGA) was carried out with Shimadzu Thermal Analyzer Japan. Under nitrogen atmosphere, the temperature range was 30–800 ℃ and the heating rate was 10 ℃/min.

2.5. Performance test of superabsorbent resin

2.5.1. Measurement of swelling behavior

In the experiment, 0.10 g sample was immersed in excessive distilled water, tap water and 0.9 wt% sodium chloride solution at room temperature for 4 h to achieve expansion equilibrium, respectively. Then the expanded sample was filtered through a 100 meshes sieve, separated from the unabsorbed water and weighed. Each data is the average of three measurements. Water absorption Q_{eq} (g/g) was calculated according to the following formula:

$$Q_{eq} = (M\text{-}M_0)/M_0 \quad (1)$$

where M_0 (g) and M (g) are the weights of the dry and swollen sample, respectively (Ashkani, Bouhendi, Kabiri, & Rostami, 2019). Q_{eq} was calculated as grams of water per gram of sample.

2.5.2. Measurement of swelling kinetics

The swelling kinetics of NaHMC-g-P (AA-co-AMPS)/laterite in distilled water was determined by following procedures: 0.10 g samples were immersed in 500 mL distilled water at a set time interval (3, 5, 10, 15, 30, 45, 60, 75, 90, 120, 150, 180, 210 and 240 min) (Chen et al., 2016). The water absorption rate of SAR was calculated according to formula (1).

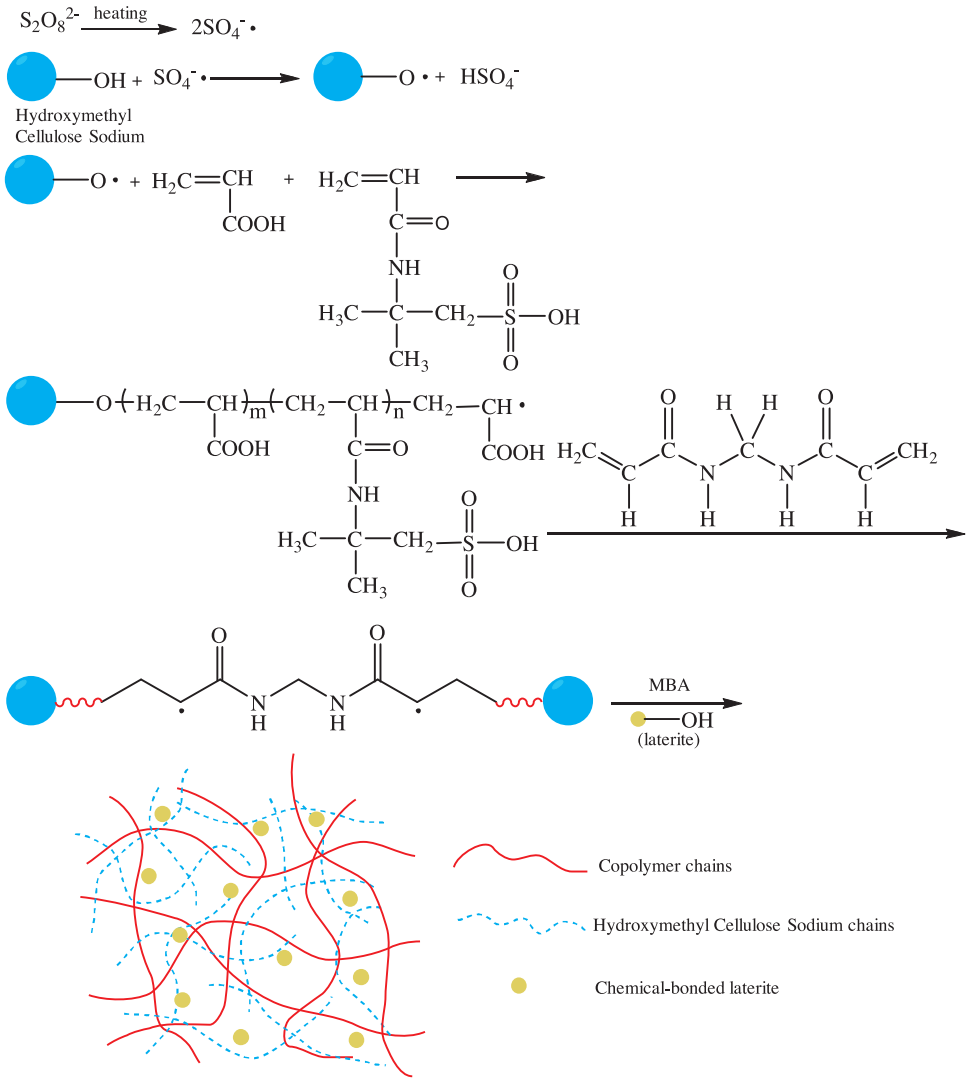

Scheme 2. The reaction mechanism for synthesis of NaHMC-g-P (AA-co-AMPS)/laterite SAR.

2.5.3. Determination of water retention at different temperatures

The 60 g swollen absorbent gel was placed at the bottom of the beaker and placed in a constant temperature blower drying chamber for 25 ℃, 35 ℃, 45 ℃ and 60 ℃ for a certain time (Zhang & Zhang, 2018b). The determination of water retention is based on the functional relationship between mass and time. The formula for calculating water retention of superabsorbent resin is as follows:

$$W_r(\%) = W_i/W_0 \times 100\% \quad (2)$$

where W_0 is the quality of completely swollen absorbent gel, and W_i is the quality of gel after a certain time at different temperatures.

2.5.4. Repeated swelling capacity test

Accurately weigh 0.1 g of dried sample and place it in 250 mL beaker. Add 200 mL distilled water (Varaprasad, Jayaramudu, & Sadiku, 2017). Stay at room temperature for 4 h to achieve swelling equilibrium. Then the fully swollen gel was placed in a 60 ℃ oven until the gel dried completely. Then, the same amount of distilled water was added to make it re-swell. The above process was repeated for several cycles, and the swelling rate was determined for each time. The calculation method is the same as 2.5.1.

2.6. The water evaporation performance test of superabsorbent resin in soil

Under natural conditions, the mass of the anti-evaporation material was weighed every 2 ~ 4 h, and data were recorded. The calculation formula of evaporation rate is as follows:

$$\text{Evaporation rate} = (M_1\text{-}M_2)/M_3 \times 100\% \quad (3)$$

in which M_1 is the total mass of the anti-evaporation material, M_2 is the mass of the anti-evaporation material when t, and M_3 is the total mass of water in the anti-evaporation material.

3. Results and discussion

3.1. FTIR results

The FTIR spectra of the NaHMC (see Fig. 1a), the absorption peaks of 1128 cm^{-1} and 1031 cm^{-1} were the C—OH bond stretching vibration (Peng, Hu et al., 2016; Peng, Wang et al., 2016), which basically disappeared after the polymerization reaction, indicating that C—OH in NaHMC was involved in chemical reaction. In the FTIR spectrum (see Fig. 1b) of AMPS, the stretching vibration absorption peak of C═O of amide group was at 1663 cm^{-1} (Huang et al., 2012), and the peak of sulfonic acid group was at 1083 cm^{-1}. The intensity of these absorption peaks decreased the FTIR spectra of the NaHMC-g-P (AA-co-AMPS), and

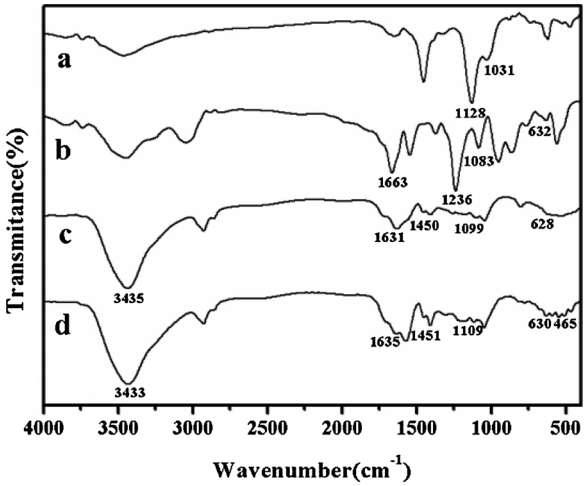

Fig. 1. FTIR spectra of (a) NaHMC, (b) AMPS, (c) NaHMC-g-P (AA-co-AMPS) and (d) NaHMC-g-P (AA-co-AMPS)/laterite (2 wt%).

NaHMC-g-P (AA-co-AMPS)/laterite (2 wt%) (see Fig. 1c and d). The absorption peak of -CN in the amide group at 1236 cm^{-1} basically disappeared after polymerization. The stretching vibration peak of O═S of sulfonic at 632 cm^{-1} shifted after polymerization (Singh & Singh, 2017). This indicated that NaHMC grafted AMPS successfully. In the Fig. 1c and d, the asymmetric stretching vibration peaks of $-COO-$ at 1456 cm^{-1} and 1411 cm^{-1} were observed respectively, indicating that the acrylic acid chain had grafted to the NaHMC skeleton. Compared with the peak at 3435 cm^{-1} in Fig. 1c, the intensity of the broad peak of O–H at 3433 cm^{-1} (Anirudhan, Tharun, & Rejeena, 2011) in Fig. 1d increased. In addition, we found the bending vibration peak of $SiO-Si$ at 465 cm^{-1} in the laterite, which indicated that the laterite participated in the graft copolymerization.

3.2. SEM results

SEM images of NaHMC, NaHMC-g-P (AA-co-AMPS) and NaHMC-g-P (AA-co-AMPS)/laterite (2 wt%) was observed and shown in Fig. 2. As can be seen from the Fig. 2, NaHMC had a smooth, tight surface and without pore structure (Yang & Cranston, 2014). The surface of NaHMC-g-P (AA-co-AMPS) and NaHMC-g-P (AA-co-AMPS)/laterite (2 wt%) showed a relatively coarse and loose structure. NaHMC-g-P (AA-co-AMPS) superabsorbent resin had partial pore structure. After the addition of laterite, the surface morphology of the superabsorbent resin has changed significantly, and the surface presented a relatively uniform pore structure, which was conducive to water penetrating into the superabsorbent resin particles rapidly (Alam & Christopher, 2018; Cuadri, Romero, Bengoechea, & Guerrero, 2017), so that the water absorption performance of the superabsorbent resin was significantly improved (Li et al., 2013).

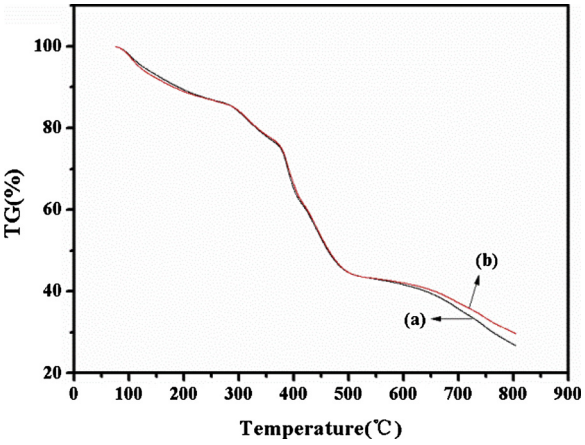

Fig. 3. Weight loss curves of (a) NaHMC-g-P (AA-co-AMPS) and (b) NaHMC-g-P (AA-co-AMPS)/laterite (2 wt%).

3.3. TGA results

TGA curves of (a) NaHMC-g-P (AA-co-AMPS) and (b) NaHMC-g-P (AA-co- AMPS)/laterite (2 wt%) were shown in Fig. 3. From it could be found that the two superabsorbent resins showed four stages of degradation (Xiao et al., 2017). Stage first stage: at 30 ~ 230 ℃, the sample weight lost about 13% of its weight, which was caused by the dehydration of the sugar ring on the NaHMC chain (Sadat Hosseini, Hemmati, & Ghaemy, 2016). Stage second stage occurred between 230 and 330 ℃, samples (a) and (b) lost 10% and 8% respectively, possibly because small molecules of the resin began to decompose. At the third stage, the weight loss of samples about 33% in the range of 330 ~ 510 ℃, are ascribed to the polymer began to decompose (Kollár et al., 2016) and the three-dimensional network structure is destroyed (Zhang, Cheng et al., 2014). Stage fourth stage ranged from 510 to 800 ℃, samples (a) and (b) lost 16% and 13%, respectively, which was due to the elimination of SO_2 molecules (Shah et al., 2018). By analyzing the weight loss of the two samples, we can draw a conclusion that the introduction of laterite during the polymerization process could improve the thermal stability of the resin, and also proved that laterite was involved in the reaction.

3.4. The effects of synthesis conditions on water (salt) absorbency of SAR

3.4.1. Effect of weight ratios of NaHMC to AA on water (salt) absorbency of SAR

AA monomer was used as a reference for the convenience of research. As can be seen from the Fig. 4(a), with the increase of NaHMC content from 8 to 20 wt% the water (salt) absorbency increased first and then decreased. The main reason was that when the content of NaHMC was less than 12 wt%, the molecular weight of the polymer was lower, the water solubility was increased. It is difficult for the resin to

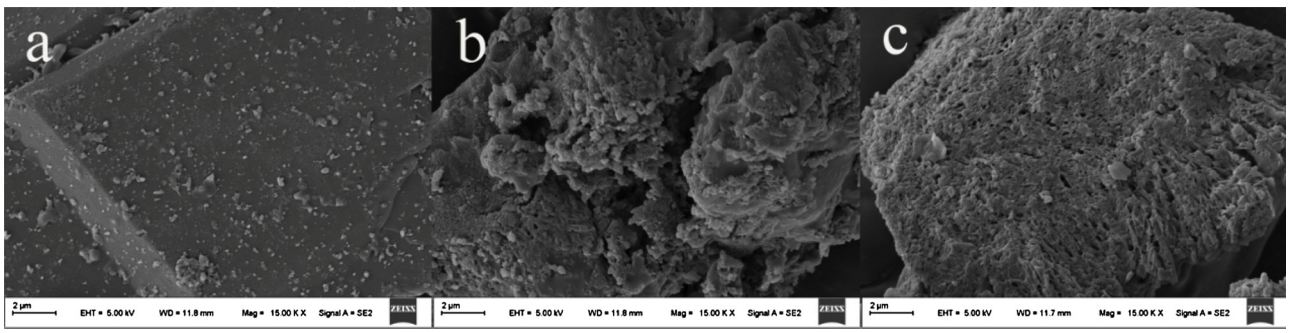

Fig. 2. Scanning electron micrographs of (a) NaHMC, (b) NaHMC-g-P (AA-co-AMPS) and (c) NaHMC-g-P (AA-co-AMPS)/laterite (2 wt%).

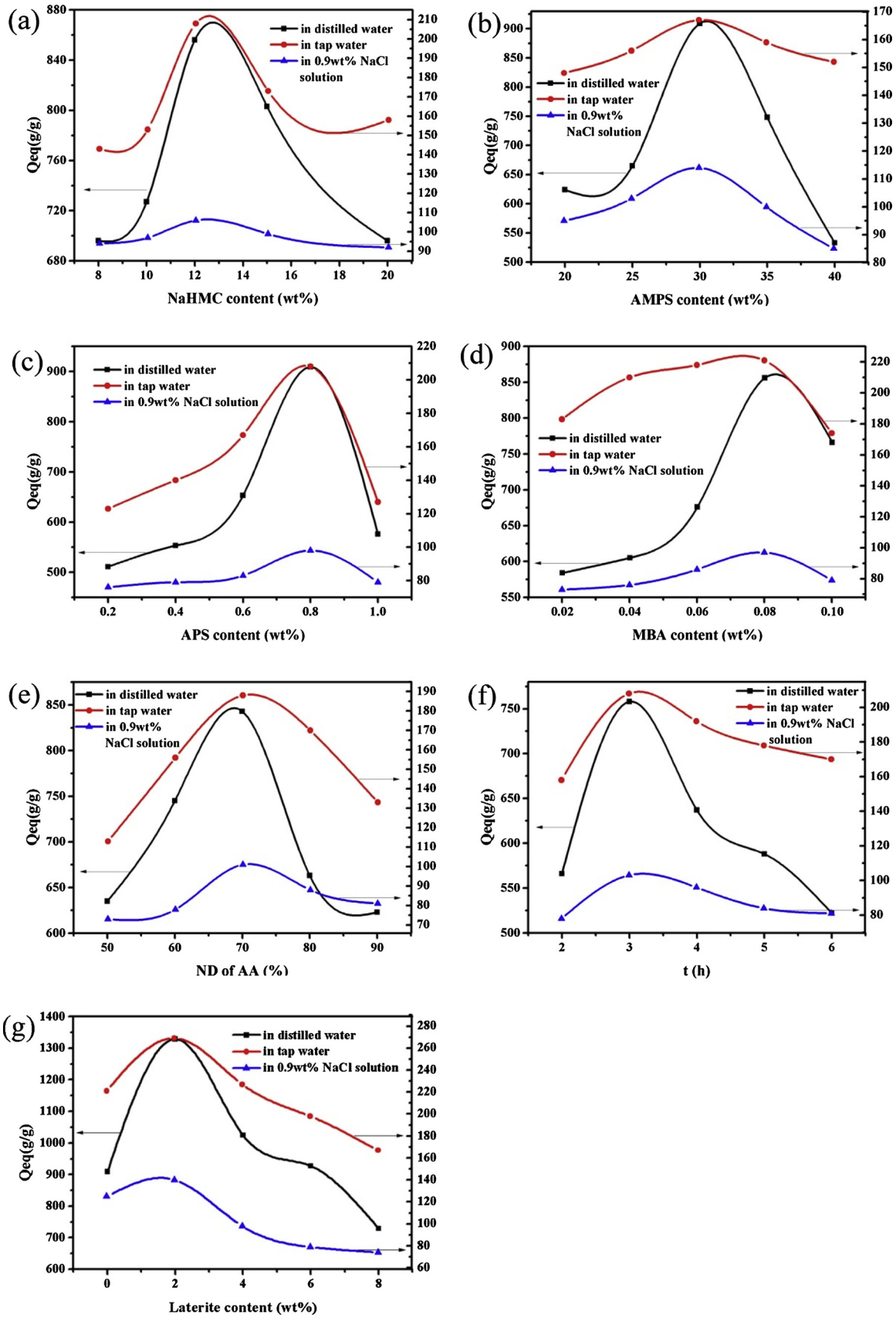

Fig. 4. The effects of synthesis conditions on water (salt) absorbency of SAR: Effect of (a) NaHMC content; (b) AMPS content; (c) APS content; (d) MBA content; (e) neutralization degree (ND) of AA; (f) reaction time and (g) laterite content on water (salt) absorbency of SAR.

form an effective network structure, which was not conducive to enhance the water (salt) absorption ability. Further increasing the content of NaHMC, the viscosity of the reaction system increased, which could hinder the collision between monomers and free radicals, reduced the reaction speed. The shortening of the branch chain was not conducive to the formation of an effective network structure, and the water (salt) absorbency of the resin showed a downward trend. Therefore, the addition of appropriate NaHMC effectively increased the molecular weight of SAR, which was conducive to enhance water (salt) absorbency of SAR (Agnihotri & Singhal, 2018). The good ductility and semi-rigidity of NaHMC main chain could further improve the expansion performance of the three-dimensional network of resins, enhance the network space, the water (salt) absorbency capacity of the resin was further increased.

3.4.2. Effect of weight ratios of AMPS to AA on water (salt) absorbency of SAR

The effect of AMPS content on the water (salt) absorbency of SAR was shown in Fig. 4(b). The results showed that the water (salt) absorbency of the resin increased first and then decreased with the increase of the content of AMPS. The main reason was that AMPS contains strong hydrophilic groups such as amide group and sulfonic group (Yang, Wang, Liu, Liu, & Hu, 2019). When an appropriate amount of AMPS was added to the reaction system, the hydrophilic groups in the polymer network increased, which improved the water (salt) absorbency ability of the resin. However, when AMPS was excessive, the steric hindrance of the reaction system increased, the reaction was incomplete, the molecular weight of SAR was reduced, and the soluble resin increased, which impeded the formation of effective network structure, and decreased the water (salt) absorbency of the product (Liu et al., 2013). When the AMPS content was 30 wt%, the resin formed a better network structure and the water (salt) absorption was the best (Fang et al., 2019).

3.4.3. Effect of initiator content on water (salt) absorbency of SAR

The effect of APS content on water (salt) absorbency was shown in Fig. 4(c). The water (salt) absorbency of superabsorbent resin varies with the increase of APS content, which was related to the relationship between the average chain length of initiator and the concentration of initiator in the process of polymerization (Liu et al., 2013). When the content of initiator was less than 0.8 wt%, the cellulose molecular skeleton could not generate free radicals sufficiently, resulted in less grafting points and less grafting monomers in the reaction system (Fang et al., 2018). Therefore, it was impossible to form a three-dimensional polymer network structure effectively, which might result in low water (salt) absorbency. As initiator content increased, more graft copolymerization took place between AA and NaHMC, which was conducive to form a stable network structure and improve water absorbency. However, excess initiator resulted in more free radicals and accelerated polymerization reaction between cellulose molecules, the length of the main chain was shortened. Therefore, the water (salt) absorbency of resin decreased.

3.4.4. Effect of cross-linker content on water (salt) absorbency of SAR

In theory, the cross-linking density is the main factor affecting the water (salt) absorbency of superabsorbent resin. The effect of MBA content, as cross-linking agent, on the water (salt) absorbency of SAR was shown in Fig. 4(d). It can be seen that increasing the content of MBA from 0.02 wt% to 0.10 wt%, the water (salt) absorbency first increased and then decreased. This result was observed that the cross-linking density increased with the increase of MBA content. When MBA content was lower than 0.08 wt%, the cross-linking density was lower, SAR would become water soluble resin after water absorbed, which led to water (salt) absorbency decreased (Huang, Liu, Fang, & Zhang, 2013). As the cross-linking density increased, more three-dimensional polymer networks with small pore size were formed, which would conducive to improve the water (salt) absorbency of SAR (Qiao et al., 2016). However, higher the concentration of MBA resulted in the cross-linking density was too high, the pore size of the three-dimensional network became smaller, and the elasticity of the resin decreased, which was responsible for the decrease of water (salt) absorbency.

3.4.5. Effect of neutralization degree of AA on water (salt) absorbency of SAR

The neutralization degree (ND) of AA is also an important factor affecting the water absorbency performance of SAR. Fig. 4(e) showed that the effect of ND of AA, neutralized with sodium hydroxide, on water (salt) absorbency. The results showed that the water (salt) absorbency of SAR increased gradually with the ND of AA from 50 to 70%, and then decreased with the ND further increasing to 90%. When ND was lower, the acidity of aqueous phase was higher and the polymerization reaction was completed quickly (Zhang & Zhang, 2018b), resulted in the formation of highly cross-linked polymers and lower water absorbency. With the increase of ND, the increase of the hydrophilic groups and Na^+ content in the composite chain, which led to the increase of the ionic strength and internal osmotic pressure of the cross-linking network, which was helpful to improve water (salt) absorbency. However, when the ND exceeded 70%, the concentration of Na^+ ions in the polymer network increased, more Na^+ ions react with COO^- groups, and the repulsion was weakened, which resulted in the water (salt) absorbency dropped (Behrouzi & Moghadam, 2018).

3.4.6. The effect of reaction time on water (salt) absorbency of SAR

As shown in Fig. 4(f), the effect of reaction time on the water (salt) absorbency of SAR was studied by changing time in the range of 1–4 h. It was found that the optimum reaction time was 3 h. These results were in accordance with the free radical reaction rule, which declared that when the reaction time was shorter, graft polymerization was incomplete and resulted in lower molecular mass of the resin and the size of network after swelling was smaller, so the water (salt) absorbency was lower (Cheng et al., 2018). As the time increasing, more cross-linking reaction happened, which promoted the formation of network structure. However, overlong reaction time could produce a lot of branched chains in the network structure, which would interweave with each other and hinder the expansion of the network structure of the resin (Huang et al., 2013). Therefore, the water (salt) absorbency of SAR decreased.

3.4.7. Effect of laterite content on water (salt) absorbency of SAR

The effect of laterite content on water (salt) absorbency was shown in Fig. 4(g). It is obvious that when the laterite content was 2 wt%, the swelling ratio of SAR was the highest, reaching 1329 g/g, 269 g/g and 140 g/g in distilled water, in tap water and in 0.9 wt% NaCl solution, respectively. When the laterite content was 8 wt%, the water absorbency of the resin was lower than the SAR without laterite. This phenomenon is mainly due to the fact that −OH in laterite could cross-link with polymer chains and participate in the construction of three-dimensional polymer network. The introduction of rigid laterite particles could reduce the winding of the grafted polymer network chain, weaken the hydrogen bond interaction between carboxyl groups in the polymer, thus reduced the degree of physical cross-linking in order to improve the polymer network (Feng, Ma, Wu, Wang, & Lei, 2014). However, when the laterite content increased from 2 wt% to 8 wt%, the water (salt) absorbency of SAR decreased gradually. This may be due to the addition of extra laterite particles increased the degree of cross-linking, and resulted in the permeability space of water molecule and water (salt) absorbency decreased. On the other hand, the superfluous laterite particles were filled in the polymer network space in the form of physical filling, which reduced the proportion of hydrophilic groups per unit volume and the swelling ratio of the material. According to the above results, the composite with laterite content of 2 wt% composite was selected to test other performances.

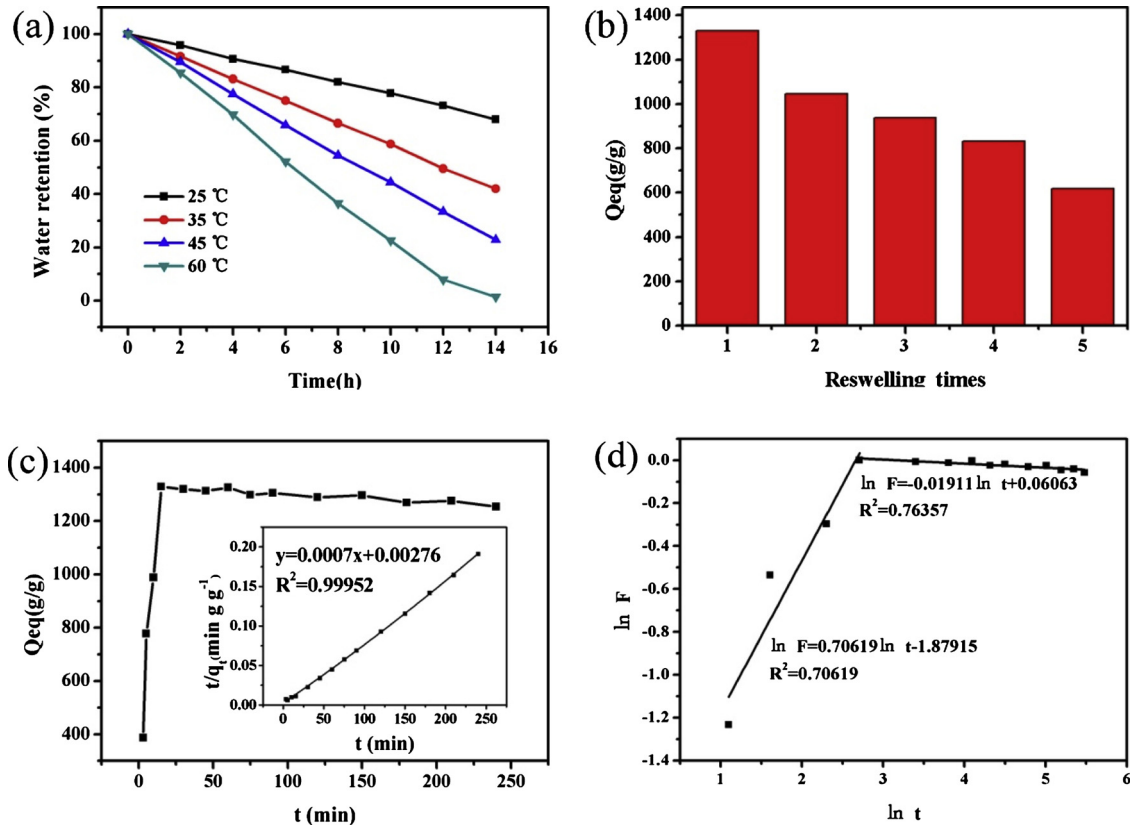

Fig. 5. (a) Water retention at different temperatures, (b) Reswelling capability, (c) and (d) Swelling kinetics of SAR (2 wt% laterite) in distilled water.

3.5. Performance tests of SAR

3.5.1. Water retention property of SAR at different temperatures

As a new type of superabsorbent resin, the water retention property at different temperatures has a great impact on its application in various fields. Therefore, the water retention property of SAR at 25, 35, 45 and 60 ℃ was investigated (Feng et al., 2014). The water retention curves were shown in Fig. 5(a). It can be seen that the water retention rate of fully swollen resin decreased with time at 25, 35, 45 and 60 ℃. The water retention curve of the resin at 25 ℃ was gentler than at higher temperature, 73.17% of water was maintained after being placed for 12 h (Zhu et al., 2012); at 35 ℃ and 45 ℃, the water retention rate was 49.5% and 33.33%, respectively; at 60 ℃, the water retention rate could reach 7.83% after 12 h. These results indicated that the composite resin has a high water retention property and can be used in practical applications.

3.5.2. Reswelling capability of SAR in distilled water

As shown in Fig. 5(b), the superabsorbent resin still had a good swelling ability after repeated use. As reswelling times increased, the water absorbency of the resin decreased, but the trend of decline slowed down, and the water absorbency could still reach about 47% of the initial value after five times of swelling-deswelling cycle (Zhang & Zhang, 2018a). This result showed that the material could be used as a material of repeated water absorption and low cost. At the same time, it also showed that the material could prolong utilization periods of the hydrogels (Gharekhani, Olad, Mirmohseni, & Bybordi, 2017).

3.5.3. Swelling kinetics of SAR in distilled water

The swelling kinetics is a crucial characteristic to describe the water absorption. The water absorption rate curve of SAR with 2 wt% laterite in distilled water was shown in Fig. 5(c) and (d). As can be seen from the Fig. 5(c), the water absorption rate of the resin was faster within 15 min and the swelling equilibrium was reached at 15 min, and it tended to be stable after 15 min (Huang et al., 2012). Based on previous reports, the swelling behavior of SAR in distilled water were evaluated by the pseudo-second-order swelling kinetics model and Ritger-Peppas model:

$$t/q_t = 1/k_2 q_e^2 + t/q_e \quad (4)$$

$$F = q_t/q_e = k \times t^n \quad (5)$$

Taking the natural logarithm of Equation:

$$\ln F = \ln q_t - \ln q_e = \ln k + n \ln t \quad (6)$$

Where q_e (g/g) and q_t (g/g) are the water absorbency of the product at equilibrium and time t, respectively. k_2 ($g \cdot mg^{-1}\,min^{-1}$) is the rate constant of the pseudo-second order model. F is the fractional uptake at time t, k is the structural parameter and n is the swelling exponent which determines the type of diffusion.

According to Fig. 5(c), the relation curve between t/q_t and t could be well linear, and the linear correlation coefficient ($R^2 = 0.99952$) is very close to 1. It showed that the pseudo-second-order swelling kinetics model had made a considerable fitting result for the swelling behavior of SAR (He et al., 2017), and the swelling kinetics of the prepared SAR was more consistent with the pseudo-second-order relationship, and had a higher correlation coefficient compared with the Ritger-Peppas model (Zhang & Zhang, 2018a). Because the pseudo-second-order kinetic model is based on chemisorption, this result indicated that the water absorption process was mainly controlled by chemical absorptions (Thakur, Pandey, & Arotiba, 2016).

For swollen hydrogel systems, the water diffusion mechanisms have been classified into five types according to the relative diffusion rate of water into polymer matrix and rate of polymer chain relaxation, $n < 0.5$, $n = 0.5$, $0.5 < n < 1$, $n = 1$ and $n > 1$ indicate pseudo-Fickian diffusion, Fickian diffusion, non-Fickian diffusion, Case II transport diffusion and relaxation diffusion, respectively (Lan et al.,

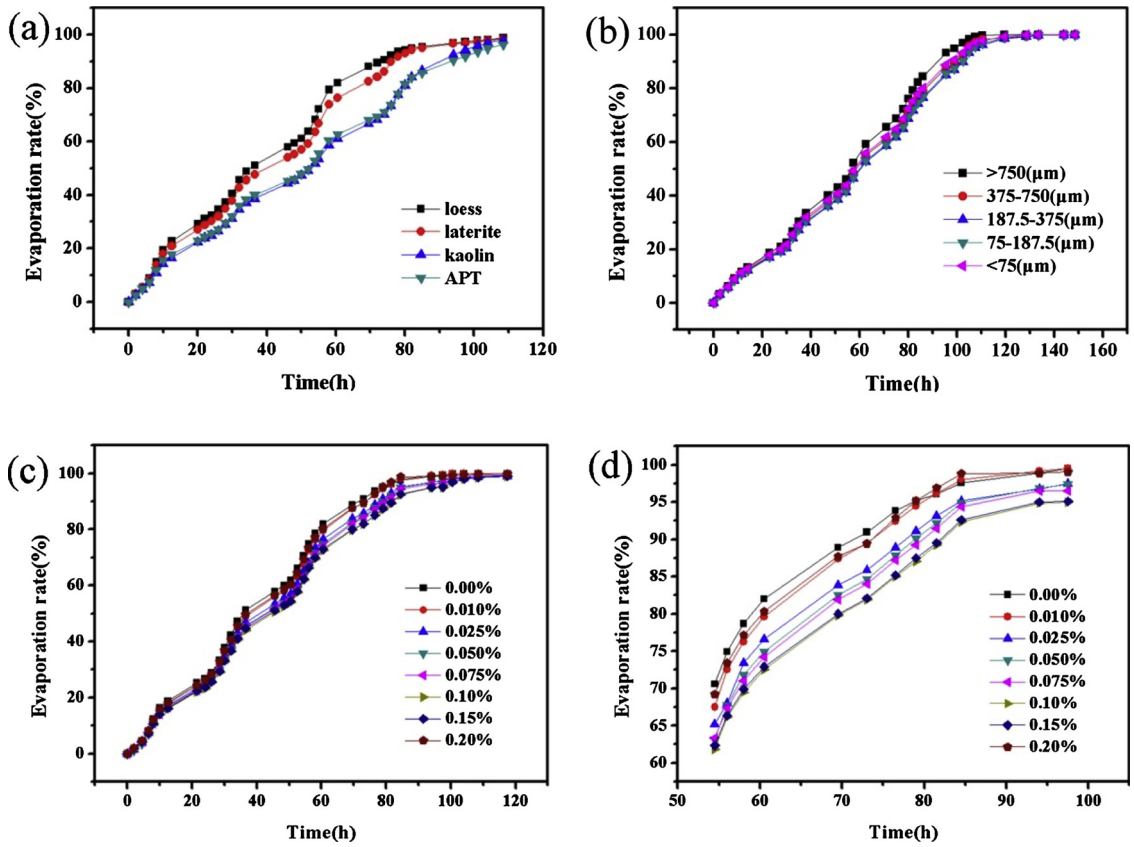

Fig. 6. Effect of (a) soil type, (b) particle size of SAR and SAR content: (c) the whole figure and (d) local enlarged figure on evaporation rate.

2019). This equation was applied to the initial stages of swelling. As shown in Fig. 5(d), in the beginning 15 min of swelling, $0.5 < n < 1$; both chain looseness and the diffusion of small molecule play a role in swelling. In non-Fickian diffusion, the diffusion and relaxation are said to be isochronally effective. 15 ~ 240 min, $n < 0.5$, the water molecule diffusion become main factor of swelling (Zhang, Wang, Li, & He, 2010).

3.5.4. Prevent water evaporation performance of SAR in soil

Fig. 6(a) showed the effect of four types of soil on the evaporation rate of the SAR. It can be seen that among the four soils, kaolin and attapulgite had lower evaporation rate, and kaolin had the best result on the whole. Therefore, we selected kaolin for subsequent experiments.

Fig. 6(b) showed the effect of particle size of the superabsorbent resin on the evaporation rate. It can be observed that the evaporation rate was relatively low when the particle size is 187.5 ~ 375 and 75 ~ 187.5 μm, and the evaporation rate is slightly lower when the particle size is 187.5 ~ 375 μm than 75 ~ 187.5 μm. Therefore, the superabsorbent resin with particle size of 187.5 ~ 375 μm was selected for follow-up experiments.

Fig. 6(c) and (d) showed the effect of the content of the superabsorbent resin on water evaporation rate in the soil. It can be seen that when the content of superabsorbent resin from 0.010% to 0.10%, the evaporation rate of the anti-evaporation material of kaolin-based superabsorbent resin decreased gradually compared with the neat soil (Essawy, Ghazy, El-Hai, & Mohamed, 2016). However, compared with the anti-evaporation material with content of 0.10% of resin, the evaporation rate increased with the resin content further increasing to 0.20%. And the evaporation rate of the anti-evaporation material with content of 0.10% of superabsorbent resin decreased by 9.49% when placed for 60.5 h under natural conditions.

In generally, we can draw the following conclusions: kaolin is selected as the type of soil, the particle size of the superabsorbent resin is 187.5 ~ 375 μm, and the material with content of 0.10% had the best anti-evaporation effect.

4. Conclusions

A series of NaHMC-g-P (AA-co-AMPS)/laterite superabsorbent resins were prepared by free radical graft copolymerization. The results showed that the optimum reaction conditions of the superabsorbent resin were that the mass of NaHMC, AMPS, APS, MBA and laterite were 12 wt%, 30 wt%, 0.8 wt%, 0.08 wt% and 2 wt% of AA, respectively. The reaction time was 3 h and the ND of AA was 70%. The maximum water absorption were 1329 g/g, 269 g/g and 140 g/g in distilled water, tap water and 0.9 wt% NaCl solution, respectively. The polymerization was confirmed by FTIR, SEM and TGA. The swelling mechanism of SAR is explained by pseudo-second-order swelling kinetics model and Ritger-Peppas model. The results showed that the swelling process of SAR is more consistent with the former. We prepared clay-based anti-evaporation materials and studied the factors affecting the water evaporation rate in soil. The results showed that when the soil type was kaolin and the particle size of the superabsorbent resin was 187.5 ~ 375 μm and the content was 0.10%, the effect of the anti-evaporation material was the best, and the evaporation rate was 9.49% lower than the neat soil. The effect of superabsorbent resin on preventing water evaporation in soil was studied in this paper, the aim is to develop new application field of superabsorbent resin.

Acknowledgements

We thank to the program for Changjiang Scholars and Innovative Research Team in University (IRT15R56), the National Natural Science Foundation of China (51863019), Key Laboratory of Eco-functional Polymer Materials of the Ministry of Education, and Key Laboratory of

Eco-Environment Polymer Materials of Gansu Province.

References

Adair, A., Kaesaman, A., & Klinpituksa, P. (2017). Superabsorbent materials derived from hydroxyethyl cellulose and bentonite: Preparation, characterization and swelling capacities. *Polymer Testing, 64*, 321–329.

Agnihotri, S., & Singhal, R. (2018). Effect of sodium alginate content in acrylic acid/sodium humate/sodium alginate superabsorbent hydrogel on removal capacity of MB and CV dye by adsorption. *Journal of Polymers and the Environment, 27*(2), 372–385.

Alam, M. N., & Christopher, L. P. (2018). Natural cellulose-chitosan cross-linked superabsorbent hydrogels with superior swelling properties. *ACS Sustainable Chemistry & Engineering, 6*(7), 8736–8742.

Anirudhan, T. S., Tharun, A. R., & Rejeena, S. R. (2011). Investigation on poly(methacrylic acid)-grafted cellulose/bentonite superabsorbent composite: Synthesis, characterization, and adsorption characteristics of bovine serum albumin. *Industrial & Engineering Chemistry Research, 50*(4), 1866–1874.

Ashkani, M., Bouhendi, H., Kabiri, K., & Rostami, M. R. (2019). Synthesis of poly (2-acrylamido-2-methyl propane sulfonic acid) with high water absorbency and absorption under load (AUL) as concrete grade superabsorbent and its performance. *Construction and Building Materials, 206*, 540–551.

Bao, Y., Ma, J., & Sun, Y. (2012). Swelling behaviors of organic/inorganic composites based on various cellulose derivatives and inorganic particles. *Carbohydrate Polymers, 88*(2), 589–595.

Behrouzi, M., & Moghadam, P. N. (2018). Synthesis of a new superabsorbent copolymer based on acrylic acid grafted onto carboxymethyl tragacanth. *Carbohydrate Polymers, 202*, 227–235.

Capanema, N. S. V., Mansur, A. A. P., de Jesus, A. C., Carvalho, S. M., de Oliveira, L. C., & Mansur, H. S. (2018). Superabsorbent crosslinked carboxymethyl cellulose-PEG hydrogels for potential wound dressing applications. *International Journal of Biological Macromolecules, 106*, 1218–1234.

Chen, W., Ma, J., Zhu, L., Morsi, Y., Ei-Hamshary, H., Al-Deyab, S. S., & Mo, X. (2016). Superelastic, superabsorbent and 3D nanofiber-assembled scaffold for tissue engineering. *Colloids and Surfaces B Biointerfaces, 142*, 165–172.

Cheng, D., Liu, Y., Yang, G., & Zhang, A. (2018). Water- and fertilizer-integrated hydrogel derived from the polymerization of acrylic acid and urea as a slow-release N fertilizer and water retention in agriculture. *Journal of Agricultural and Food Chemistry, 66*(23), 5762–5769.

Cuadri, A. A., Romero, A., Bengoechea, C., & Guerrero, A. (2017). Natural superabsorbent plastic materials based on a functionalized soy protein. *Polymer Testing, 58*, 126–134.

Demeter, M., Virgolici, M., Vancea, C., Scarisoreanu, A., Kaya, M. G. A., & Meltzer, V. (2017). Network structure studies on γ–irradiated collagen–PVP superabsorbent hydrogels. *Radiation Physics and Chemistry, 131*, 51–59.

Essawy, H. A., Ghazy, M. B., El-Hai, F. A., & Mohamed, M. F. (2016). Superabsorbent hydrogels via graft polymerization of acrylic acid from chitosan-cellulose hybrid and their potential in controlled release of soil nutrients. *International Journal of Biological Macromolecules, 89*, 144–151.

Fang, S., Wang, G., Li, P., Xing, R., Liu, S., Qin, Y., ... Li, K. (2018). Synthesis of chitosan derivative graft acrylic acid superabsorbent polymers and its application as water retaining agent. *International Journal of Biological Macromolecules, 115*, 754–761.

Fang, S., Wang, G., Xing, R., Chen, X., Liu, S., Qin, Y., ... Li, P. (2019). Synthesis of superabsorbent polymers based on chitosan derivative graft acrylic acid-co-acrylamide and its property testing. *International Journal of Biological Macromolecules, 132*, 575–584.

Feng, E., Ma, G., Wu, Y., Wang, H., & Lei, Z. (2014). Preparation and properties of organic-inorganic composite superabsorbent based on xanthan gum and loess. *Carbohydrate Polymers, 111*, 463–468.

Gharekhani, H., Olad, A., Mirmohseni, A., & Bybordi, A. (2017). Superabsorbent hydrogel made of NaAlg-g-poly(AA-co-AAm) and rice husk ash: Synthesis, characterization, and swelling kinetic studies. *Carbohydrate Polymers, 168*, 1–13.

Guilherme, M. R., Aouada, F. A., Fajardo, A. R., Martins, A. F., Paulino, A. T., Davi, M. F. T., ... Muniz, E. C. (2015). Superabsorbent hydrogels based on polysaccharides for application in agriculture as soil conditioner and nutrient carrier: A review. *European Polymer Journal, 72*, 365–385.

He, G., Ke, W., Chen, X., Kong, Y., Zheng, H., Yin, Y., & Cai, W. (2017). Preparation and properties of quaternary ammonium chitosan-g-poly(acrylic acid-co-acrylamide) superabsorbent hydrogels. *Reactive & Functional Polymers, 111*, 14–21.

Hosseinzadeh, H., & Ramin, S. (2016). Magnetic and pH-responsive starch-g-poly(acrylic acid-coacrylamide)/graphene oxide superabsorbent nanocomposites: One-pot synthesis, characterization, and swelling behavior. *Starch – Stärke, 68*(3–4), 200–212.

Huang, Y., Zeng, M., Ren, J., Wang, J., Fan, L., & Xu, Q. (2012). Preparation and swelling properties of graphene oxide/poly(acrylic acid-co-acrylamide) super-absorbent hydrogel nanocomposites. *Colloids and Surfaces A: Physicochemical and Engineering Aspects, 401*, 97–106.

Huang, Z., Liu, S., Fang, G., & Zhang, B. (2013). Synthesis and swelling properties of beta-cyclodextrin-based superabsorbent resin with network structure. *Carbohydrate Polymers, 92*(2), 2314–2320.

Kang, S.-H., Hong, S.-G., & Moon, J. (2017). Absorption kinetics of superabsorbent polymers (SAP) in various cement-based solutions. *Cement and Concrete Research, 97*, 73–83.

Kollár, J., Mrlík, M., Moravčíková, D., Kroneková, Z., Liptaj, T., Lacík, I., & Mosnáček, J. (2016). Tulips: A renewable source of monomer for superabsorbent hydrogels. *Macromolecules, 49*(11), 4047–4056.

Lan, G., Zhang, M., Liu, Y., Qiu, H., Xue, S., Zhang, T., & Xu, Q. (2019). Synthesis and swelling behavior of super-absorbent soluble Starch-g-poly(AM-co-NaAMC$_{14}$S) through graft copolymerization and hydrolysis. *Starch – Stärke*1800272.

Li, Q., Lu, H., Xiao, H., Gao, K., & Diao, M. (2013). Adsorption capacity of superabsorbent resin composite enhanced by non-thermal plasma and its adsorption kinetics and isotherms to lead ion in water. *Journal of Environmental Chemical Engineering, 1*(4), 996–1003.

Liu, J., Li, Q., Su, Y., Yue, Q., Gao, B., & Wang, R. (2013). Synthesis of wheat straw cellulose-g-poly (potassium acrylate)/PVA semi-IPNs superabsorbent resin. *Carbohydrate Polymers, 94*(1), 539–546.

Mechtcherine, V., Snoeck, D., Schröfl, C., De Belie, N., Klemm, A. J., Ichimiya, K., ... Falikman, V. (2018). Testing superabsorbent polymer (SAP) sorption properties prior to implementation in concrete: Results of a RILEM Round-Robin Test. *Materials and Structures, 51*(1).

Olad, A., Gharekhani, H., Mirmohseni, A., & Bybordi, A. (2017). Synthesis, characterization, and fertilizer release study of the salt and pH-sensitive NaAlg-g-poly(AA-co-AAm)/RHA superabsorbent nanocomposite. *Polymer Bulletin, 74*(8), 3353–3377.

Peng, N., Hu, D., Zeng, J., Li, Y., Liang, L., & Chang, C. (2016). Superabsorbent cellulose–Clay nanocomposite hydrogels for highly efficient removal of dye in water. *ACS Sustainable Chemistry & Engineering, 4*(12), 7217–7224.

Peng, N., Wang, Y., Ye, Q., Liang, L., An, Y., Li, Q., & Chang, C. (2016). Biocompatible cellulose-based superabsorbent hydrogels with antimicrobial activity. *Carbohydrate Polymers, 137*, 59–64.

Qiao, D., Liu, H., Yu, L., Bao, X., Simon, G. P., Petinakis, E., & Chen, L. (2016). Preparation and characterization of slow-release fertilizer encapsulated by starch-based superabsorbent polymer. *Carbohydrate Polymers, 147*, 146–154.

Qin, B., Dou, G., Wang, Y., Xin, H., Ma, L., & Wang, D. (2017). A superabsorbent hydrogel–ascorbic acid composite inhibitor for the suppression of coal oxidation. *Fuel, 190*, 129–135.

Sadat Hosseini, M., Hemmati, K., & Ghaemy, M. (2016). Synthesis of nanohydrogels based on tragacanth gum biopolymer and investigation of swelling and drug delivery. *International Journal of Biological Macromolecules, 82*, 806–815.

Salmawi, K. M. E., El-Naggar, A. A., & Ibrahim, S. M. (2018). Gamma irradiation synthesis of carboxymethyl cellulose/acrylic acid/clay superabsorbent hydrogel. *Advances in Polymer Technology, 37*(2), 515–521.

Shah, L. A., Khan, M., Javed, R., Sayed, M., Khan, M. S., Khan, A., & Ullah, M. (2018). Superabsorbent polymer hydrogels with good thermal and mechanical properties for removal of selected heavy metal ions. *Journal of Cleaner Production, 201*, 78–87.

Singh, B., & Singh, B. (2017). Influence of graphene-oxide nanosheets impregnation on properties of sterculia gum-polyacrylamide hydrogel formed by radiation induced polymerization. *International Journal of Biological Macromolecules, 99*, 699–712.

Thakur, S., Pandey, S., & Arotiba, O. A. (2016). Development of a sodium alginate-based organic/inorganic superabsorbent composite hydrogel for adsorption of methylene blue. *Carbohydrate Polymers, 153*, 34–46.

Varaprasad, K., Jayaramudu, T., & Sadiku, E. R. (2017). Removal of dye by carboxymethyl cellulose, acrylamide and graphene oxide via a free radical polymerization process. *Carbohydrate Polymers, 164*, 186–194.

Wang, F., Yang, J., Cheng, H., Wu, J., & Liang, X. (2015). Study on mechanism of desorption behavior of saturated superabsorbent polymers in concrete. *ACI Materials Journal, 112*(3).

Wang, Z., Ning, A., Xie, P., Gao, G., Xie, L., Li, X., & Song, A. (2017). Synthesis and swelling behaviors of carboxymethyl cellulose-based superabsorbent resin hybridized with graphene oxide. *Carbohydrate Polymers, 157*, 48–56.

Xiao, X., Yu, L., Xie, F., Bao, X., Liu, H., Ji, Z., & Chen, L. (2017). One-step method to prepare starch-based superabsorbent polymer for slow release of fertilizer. *Chemical Engineering Journal, 309*, 607–616.

Yang, J., Wang, F., Liu, Z., Liu, Y., & Hu, S. (2019). Early-state water migration characteristics of superabsorbent polymers in cement pastes. *Cement and Concrete Research, 118*, 25–37.

Yang, X., & Cranston, E. D. (2014). Chemically cross-linked cellulose nanocrystal aerogels with shape recovery and superabsorbent properties. *Chemistry of Materials, 26*(20), 6016–6025.

Zhang, J.-P., & Zhang, F.-S. (2018a). A new approach for blending waste plastics processing: Superabsorbent resin synthesis. *Journal of Cleaner Production, 197*, 501–510.

Zhang, J.-P., & Zhang, F.-S. (2018b). Recycling waste polyethylene film for amphoteric superabsorbent resin synthesis. *Chemical Engineering Journal, 331*, 169–176.

Zhang, M., Cheng, Z., Zhao, T., Liu, M., Hu, M., & Li, J. (2014). Synthesis, characterization, and swelling behaviors of salt-sensitive maize bran-poly(acrylic acid) superabsorbent hydrogel. *Journal of Agricultural and Food Chemistry, 62*(35), 8867–8874.

Zhang, Y., Liang, X., Yang, X., Liu, H., & Yao, J. (2014). An eco-friendly slow-release urea fertilizer based on waste mulberry branches for potential agriculture and horticulture applications. *ACS Sustainable Chemistry & Engineering, 2*(7), 1871–1878.

Zhang, Y., Wang, L., Li, X., & He, P. (2010). Salt-resistant superabsorbents from inverse-suspension polymerization of PEG methacrylate, acryamide and partially neutralized acrylic acid. *Journal of Polymer Research, 18*(2), 157–161.

Zhu, D., Bai, B., & Hou, J. (2017). Polymer gel systems for water management in high-temperature petroleum reservoirs: A chemical review. *Energy & Fuels, 31*(12), 13063–13087.

Zhu, Z.-Q., Sun, H.-X., Qin, X.-J., Jiang, L., Pei, C.-J., Wang, L., & Deng, W.-Q. (2012). Preparation of poly(acrylic acid)–graphite oxide superabsorbent nanocomposites. *Journal of Materials Chemistry, 22*(11), 4811.